RSC Advances

PAPER

View Article Online
View Journal | View Issue

Cite this: *RSC Adv.*, 2022, **12**, 28804

Formation and evolution of C–C, C–O, C=O and C–N bonds in chemical reactions of prebiotic interest†

Alejandro Arias, [a] Sara Gómez, *[b] Natalia Rojas-Valencia, [ac] Francisco Núñez-Zarur, [d] Chiara Cappelli, [b] Juliana A. Murillo-López [e] and Albeiro Restrepo *[a]

Received 22nd September 2022
Accepted 27th September 2022

DOI: 10.1039/d2ra06000k

rsc.li/rsc-advances

A series of prebiotic chemical reactions yielding the precursor building blocks of amino acids, proteins and carbohydrates, starting solely from HCN and water is studied here. We closely follow the formation and evolution of the pivotal C–C, C–O, C=O, and C–N bonds, which dictate the chemistry of the molecules of life. In many cases, formation of these bonds is set in motion by proton transfers in which individual water molecules act as catalysts so that water atoms end up in the products. Our results indicate that the prebiotic formation of carbon dioxide, formaldehyde, formic acid, formaldimine, glycolaldehyde, glycine, glycolonitrile, and oxazole derivatives, among others, are best described as highly nonsynchronous concerted single step processes. Nonetheless, for all reactions involving double proton transfer, the formation and breaking of O–H bonds around a particular O atom occur in a synchronous fashion, apparently independently from other primitive processes. For the most part, the first process to initiate seems to be the double proton transfer in the reactions where they are present, then bond breaking/formation around the reactive carbon in the carbonyl group and finally rupture of the C–N bonds in the appropriate cases, which are the most reluctant to break. Remarkably, within the limitations of our non-dynamical computational model, the wide ranges of temperature and pressure in which these reactions occur, downplay the problematic determination of the exact constraints on the early Earth.

1 Introduction

Abiogenesis, or the origins of life starting from non living matter, is a rich, interdisciplinary field of research encompassing work from areas as diverse as chemistry, physics, biology, astronomy, geology, among others;[1–3] its ultimate goal is to determine the conditions and mechanisms that allow life to emerge. Prebiotic chemistry, specifically, seeks to determine what type of chemical compounds and chemical reactions are necessary to produce the constituent components of life, such as biomolecules, and also studies the set of networks of chemical reactions capable of sustaining life as we know it, whether these processes took place on the early Earth, or elsewhere in the interstellar medium.[4,5] One progressive reductionist view (life → biology → chemistry → physics → mathematics) is that the emergence of life is a deterministic process, governed by scientific laws, which only needs long times and appropriate local conditions so that isolated events with tiny probabilities do eventually occur and by virtue of local evolution (molecular or otherwise), accumulate and originate highly improbable systems.

There are several hypotheses on how life originated, prioritizing either metabolism, self-replication, or a combination of both.[6–10] In the RNA world hypothesis, RNA acted as information storage, replicator, and as an active catalyst.[11–13] Other views argue in favor of RNA cooperating with peptides and other biomolecules.[14] The metabolism-first hypothesis posits that the first living organisms appeared as the final steps of the evolution towards increasing complexity of networks of sequential chemical reactions aided by simple metal catalysts.[10,15] The molecules of life (water, carbohydrates, proteins, nucleic acids, ATP, *etc.*) contain only a few types of atoms, most prominently hydrogen, carbon, oxygen, nitrogen, sulfur, phosphorous. Consequently, any rationalization of how those large

[a]*Instituto de Química, Universidad de Antioquia UdeA, Calle 70 No. 52-21, Medellín, Colombia. E-mail: albeiro.restrepo@udea.edu.co*

[b]*Scuola Normale Superiore, Classe di Scienze, Piazza dei Cavalieri 7, Pisa, 56126, Italy. E-mail: sara.gomezmaya@sns.it*

[c]*Escuela de Ciencias y Humanidades, Departamento de Ciencias Básicas, Universidad Eafit, Medellín, AA 3300, Colombia*

[d]*Facultad de Ciencias Básicas, Universidad de Medellín, Carrera 87 No. 30-65, Medellín, 050026, Colombia*

[e]*Departamento de Ciencias Químicas, Facultad de Ciencias Exactas, Universidad Andres Bello, Autopista, Concepción-Talcahuano, Talcahuano 7100, Chile*

† Electronic supplementary information (ESI) available: Cartesian coordinates for all isolated reactants, long range complexes, transition states, and products. Gibbs activation and reaction energies in gas phase and in solution for the set of 23 reactions are provided. Plots of absolute and intrinsic activation energies for reactions **10**, **12**, **17** over grids of temperature and pressure. Plots of the natural charges at all oxygen atoms for followed along the entire IRC of reaction **3**. See https://doi.org/10.1039/d2ra06000k

biomolecules came to be, at least on Earth, must include detailed descriptions of the formation of C–C, C=O, C–O and C–N bonds and of the formation of the small molecules that act as the initial building blocks in the series of chemical reactions affording such complicated primary sequences from primitive environments, presumably rich in one carbon (C1) molecules.[1] One of those C1 molecules, abundant in extreme environments such as the interstellar medium, planetary and lunar atmospheres within our own solar system, comets, and in the conditions of the primitive Earth is HCN,[16–19] which is a favorite target for the ultimate precursor of biomolecules.[20–23] Recently, Das and coworkers,[15] starting with binary mixtures of water and HCN, offered *via* molecular dynamics simulations in *ab initio* nanoreactors, a detailed picture of the myriad of chemical reactions leading to small molecules that are the building blocks of most large biomolecules, i. e., carbon dioxide CO_2, formaldehyde CH_2O, formic acid H_2CO_2, formaldimine CH_3N, glycolaldehyde $C_2H_4O_2$, glycine $C_2H_5NO_2$, glycolonitrile C_2H_3NO, oxazole C_3H_3NO derivatives, among many others.

The scientific literature cited above has provided detailed mechanistic pathways identifying reactants, transition states, intermediates, and products as well as estimating the energetics of the chemical reactions that result in the formation of the target molecules building biochemical complexity. Sadly, crucial knowledge describing the formation of the all important C–C, C–O, C=O, and C–N bonds from the perspective of primitive changes is found nowhere. Consequently, in this work, building on the results of Das,[15] we have studied a network of reaction mechanisms yielding the experimentally reported precursor molecules of RNA and proteins. To that end, we closely follow the evolution of bonding interactions leading to formal bonds along the intrinsic reaction coordinates using the tools provided by the Quantum Theory of Atoms in Molecules (QTAIM)[24–26] and the Natural Bond Orbitals (NBO).[27–29] At this point, it is important to mention that we use QTAIM and NBO as formal analysis tools and make no attempt at discussing their merits and flaws, for which the reader is referred to the extensive literature. The combination of NBO, QTAIM, and other descriptors of bonding allows a detailed dissection of reaction mechanisms and has proven to be an enormously valuable tool to gain insight into the evolution of chemical bonds. A variety of reactions has been successfully studied in the past by our group using this methodology.[30–37]

2 Computational methods

Reaction paths starting with HCN and H_2O and linking the set of molecular precursors of large biomolecules listed above, i. e., carbon dioxide, formaldehyde, formic acid, formaldimine, glycolaldehyde, glycine, glycolonitrile, and oxazole derivatives, were determined both in gas phase and in aqueous medium, as modelled by the Polarizable Continuum Model (PCM) approach[38,39] *via* intrinsic reaction coordinate (IRC) calculations using second order Moller–Plesset perturbation theory at the MP2/6-311++G(d, p) level. The latter is chosen so that the ambiguity and non systematic problems in the treatment of electron correlation and dispersion proper of Density Functional Theory (DFT) methods are eliminated. All stationary points within a given Potential Energy Surface (PES) were characterized as true minima or saddle points *via* harmonic vibrational analysis at the same level.

We study the energetics of the entire set of 23 reactions listed in Table 1 and characterized every single reactant, product, intermediate, and transition state. However, because of the large number of intermediates and chemical reactions, in order to study the evolution of chemical bonding, we chose a set of five reactions that are particularly relevant in the complex reacting system. These reactions happen to be essential in the pathway towards the target products, which can not be obtained unless those reactions are considered. The point is, the formation of formic acid from HCN and water is the common root from where chemistry branches out into several other intermediates and products according to the following sequence of reactions:

1. HCN + H_2O $\rightarrow\cdots\rightarrow$ HCOOH (formic acid). Reaction **3** is the last step of this series.

2. HCOOH $\rightarrow\cdots\rightarrow$ H_2CO (formaldehyde). Reaction **10** is the last step of this series.

3. H_2CO + NH_3 $\rightarrow$ CH_5NO (methanol amine *via* reaction **12**).

4. CH_5NO $\rightarrow\cdots\rightarrow$ $C_2H_5NO_2$ (glycine). Reaction **17** is the last step of this series.

5. CH_2O + HNC $\rightarrow$ C_2H_3NO (glycolonitrile *via* reaction **11**).

Notice that all those intermediates (formic acid (reaction **10**), formaldehyde (reaction 3), glycolonitrile (reaction **11**), amino methanol (reaction **12**)) have been experimentally reported to be precursors en route to the target molecules. Glycine is quite important because it is the only amino acid obtained in the entire reacting system. The chosen reactions enable the analysis of the formation and breaking of the very important C–O, C=O, C–C and C–N bonds starting from C1 molecules. These bonds dictate the chemistry in all the molecules of life. Scheme 1 summarizes the reasons for choosing the set of five reactions listed above as follows: formic acid leads to the formation of formaldehyde. Formaldehyde triggers competitive reactions towards glycine (Strecker synthesis of amino acids) in one channel and glycolonitrile in another. Glycolonitrile yields two further reaction paths, one leading to the oxazole derivative and the other to the glycolaldehyde sugar.

IRCs are conveniently dissected by the critical points of the reaction force, defined, as for any conservative system, as the points for which the negative derivative of the potential energy along the reaction coordinate vanishes ($F = -\mathrm{d}V/\mathrm{d}\xi = 0$).[40–43] For a given elementary step, three critical points are obtained, corresponding to reactants (ξ_R), transition state (ξ_{TS}), and products (ξ_P); the critical points of the reaction force yield the activated reactants (ξ_{R^*}) and activated products (ξ_{P^*}). These five points along the IRC are the limits of three well defined regions, namely, the reactants region, associated to the structural changes needed to bring the reactants into the geometries needed for the reaction to occur and covering the $\xi_R \rightarrow \xi_{R^*}$ interval, the transition state region, the region where most of the electron activity needed for bond breaking/formation takes place, covering the $\xi_R \rightarrow \xi_{P^*}$ interval, and the products region, where the activated products suffer further structural changes

Table 1 Absolute activation and reaction energies for our 23 elementary steps at 373 K and 1 atm, in kcal mol^{-1} units[a]

		$\Delta G^{\ddagger}_{act}$		ΔG_{rxn}	
Label	Reaction	In gas phase	In solution	In gas phase	In solution
1	$HCN + H_2O \rightarrow CH_3NO$	57.2	63.8	14.3	17.0
2	$CH_3NO \rightarrow CH_3NO$	12.9	15.9	−12.0	−14.1
3	$CH_3NO + H_2O \rightarrow NH_3 + CH_2O_2$	55.9	58.5	2.4	5.3
4*	$CH_2O_2 + HNC \rightarrow C_2HNO + H_2O$	69.9	68.2	28.6	27.9
5*	$C_2HNO \rightarrow CO + HCN$	34.6	27.3	−38.0	−38.2
6	$CO + H_2O \rightarrow CH_2O_2$	75.7	76.2	54.6	53.7
7	$HCN \rightarrow HNC$	58.0	48.8	18.4	17.7
8	$CH_2O_2 \rightarrow CO_2 + H_2$	52.9	53.1	−21.8	−16.0
9	$CH_2O_2 + H_2 \rightarrow CH_4O_2$	64.3	61.1	4.9	6.9
10	$CH_4O_2 \rightarrow CH_2O + H_2O$	35.6	37.4	−5.9	−8.5
11*	$CH_2O + HNC \rightarrow C_2H_3NO$	31.9	32.4	−20.8	−19.8
12	$CH_2O + NH_3 \rightarrow CH_5NO$	44.6	39.1	4.4	6.6
13	$CH_5NO \rightarrow CH_3N + H_2O$	40.8	39.6	−2.8	−5.4
14*	$CH_3N + HNC \rightarrow C_2H_4N_2$	NA	10.6	NA	−27.2
14	$CH_3N + HCN \rightarrow C_2H_4N_2$	39.8	NA	11.2	NA
15	$C_2H_4N_2 + H_2O \rightarrow C_2H_6N_2O$	57.5	63.8	14.8	19.0
16	$C_2H_6N_2O \rightarrow C_2H_6N_2O$	11.4	14.5	−12.8	−14.8
17	$C_2H_6N_2O + H_2O \rightarrow C_2H_5NO_2$	53.7	57.3	1.4	1.2
18	$C_2H_3NO + CH_2O \rightarrow C_3H_5NO_2$	64.5	60.4	−2.8	−1.5
19*	$C_3H_5NO_2 \rightarrow C_2H_4O_2 + HNC$	37.1	31.5	19.6	17.2
20	$C_2H_3NO + CH_3NO \rightarrow C_3H_6N_2O_2$	40.4	47.3	20.6	24.8
21	$C_3H_6N_2O_2 + HCN \rightarrow C_4H_7N_3O_2$	59.3	58.4	15.2	14.0
22	$C_4H_7N_3O_2 \rightarrow C_4H_7N_3O_2$	44.5	40.0	−9.4	−9.0
23	$C_4H_7N_3O_2 \rightarrow C_4H_5N_3O + H_2O$	35.3	37.0	−9.8	−13.1

[a] See Table S1 in the ESI for the intrinsic barriers. An asterisk attached to a label means that HNC is involved instead of HCN. Notice that reaction **14** leads to different products than those reported by Das and coworkers[15] in gas phase.

to finally release the products, covering the $\xi_P \rightarrow \xi_{P^*}$ interval. The chemical potential along the reaction path is obtained as half the sum of the energies of the HOMO and LUMO orbitals at each point of the IRC,[44,45] and the reaction electron flux (REF), is calculated as the derivative of the chemical potential along the entire reaction path.[46–48]

The evolution of bonding interactions was followed using the set of descriptors provided by QTAIM and by NBO and the

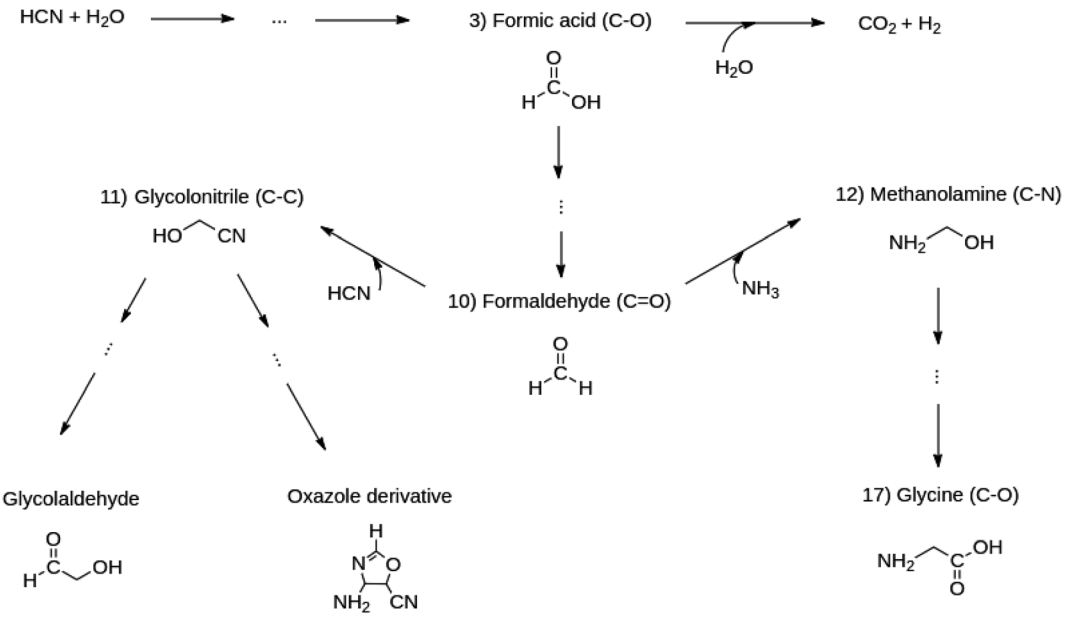

Scheme 1 The set of five reactions (reactions **3**, **10**, **11**, **12**, **17**) branching out from formic acid, chosen from Table 1, to study the formation and evolution of the C–C, C–N, C–O and C=O bonds.

recently developed GGR synchronicity index.[35] *In lieu* of a detailed description and to spare the technical details of how QTAIM and NBO descriptors are related to bonding, the interesting reader is directed to the specialized literature,[24–29] more explicitly, to the work of Rojas-Valencia *et al.*[49] (their Table 2 and the ensuing description) and references within. All electronic structure calculations including optimization, vibrational frequencies, solvent effects and IRCs were conducted using the Gaussian09 suite of programs.[50] QTAIM quantities were derived from the AIMAll suite.[51] NBO descriptors were obtained from NBO6 (ref. 52) as implemented in Gaussian.

3 Results and discussion

3.1 Reaction profiles

Starting from HCN and H_2O, production of carbon dioxide, formaldehyde, formic acid, formaldimine, glycolaldehyde, glycine, glycolonitrile and oxazole derivatives involves a total of 23 elementary steps detailed in Table 1. Subtle differences between our results and those reported by Das and coworkers[15] emerge in the HCN/HNC exchange in reactions **4**, **5**, **11**, **19** and **14**, these, however, have little consequences for the prebiotic chemistry because both species are thought to have existed in the primitive Earth reacting environment. Every single step involving more than one reactant starts with a barrier-less formation of a long range reactive complex. In this context we refer to intrinsic (reactive complex → TS) and absolute (isolated reactants → TS) activation barriers. Discrepancies between gas phase and continuum solvent activation energies are due to a stabilizing/destabilizing effect of the solvent without drastically changing the structure.

There is a high degree of uncertainty on the conditions of Hadean Earth,[53–57] with estimates ranging from very low pressures to well in excess of 20 atm and with equally unconfirmed temperatures, thus, in this work, the energetic balance of the reactions as well as the associated full and intrinsic barriers are reported as changes in the Gibbs free energies within bidimensional grids of pressure and temperature. Accordingly, an exhaustive study of the dependency of activation energies with temperatures and pressures over a grid of [293 373] K and [0.5,20] atm was carried out, the results for elementary steps **3** and **11** leading to formic acid and glycolonitrile (Table 1) are shown in Fig. 1, additional plots are provided in the in the ESI (Fig. S1 and S2†). A few important points are immediately drawn. First, only moderate changes in activation energies as a function *P*, *T* are observed. This is a very important observation because given the current poor knowledge of primitive conditions, our calculations indicate that once the thresholds for these conditions are overcome,[9] then the chemical reactions will occur under a wide variety of conditions. Second, activation energies are relatively high and not too far from the DFT calculations of Das and coworkers, nonetheless, a few of the calculated energy barriers are low enough to be encouraging about the feasibility of these processes to occur.[58–60] In any case, all these processes would greatly benefit from natural catalysts such as clays and metal surfaces, which have been postulated to be pivotal components of prebiotic chemistry.[61–64]

The Gibbs activation barriers listed in Table 1 lead to slow processes, yet these reactions must be thermodynamic and kinetically viable to be considered as part of likely mechanisms for the formation of life building blocks in prebiotic conditions. These energetic and kinetic observations, in addition to the extreme complexity offered by the *ab initio* nanoreactor, suggest a more efficient production of the precursors studied in this work under catalytic environments, which are not considered in this work. Notwithstanding, our approach offers valuable insight to understand the bonding interactions driving the reaction mechanisms and should be considered a stepping stone to explicitly deal with the role of catalysts, work that is already in progress in our group.

Several of the reactions under discussion have been already studied with various forms of catalysts, which have proven to significantly reduce activation barriers. For example, Krug *et al.* studied the hydrolysis of formamide (reaction **3**) under basic and acidic catalysis, and obtained a 6 kcal mol^{-1} barrier for the N-protonated case, 19 kcal mol^{-1} for the basic promoted case, and a stepwise mechanism for the O-protonated case, with two barriers of 24 and 16 kcal mol^{-1} for the nucleophilic addition to C and the breaking of the C–N bond respectively.[65] Thus, significant reductions of the barriers were found when compared to the neutral case, which afforded a 44 kcal mol^{-1} barrier. These environment dependent catalysis are relevant since the exact pH under prebiotic conditions is unknown, with estimates pointing to non-neutral scenarios.[66] Ice has also been suggested as a proper catalyst in prebiotic conditions. Despite the lack of a universally accepted geochemical model for the primitive earth, well grounded geochemical models that call for the presence of stable icy environments have been proposed.[67–70] The icy protons allow the so called "proton-relay" mechanism to take place,[71,72] in which a network of hydrogen bonded water molecules present in the ice surface assist in the proton transfer required in most of the set of 23 reactions listed in Table 1. Rimola *et al.* successfully assessed the catalytic effect of ice in the well known Strecker synthesis of amino acids, reporting barriers of 9.6, 21.3, and 8–9 kcal mol^{-1} for reactions **12**, **13** and **14** respectively.[73] Our isolated gas phase calculations are in agreement with their results.

Reaction **3**, the neutral hydrolysis of formamide, which we will use to dissect and highlight mechanistic trends in the set of studied prebiotic reactions, has been studied before in the gas phase and in solution with explicit consideration of either one single water molecule as reactant or assisted by an extra water molecule as catalyst.[65,74–76] Stepwise and concerted mechanisms have been reported. After refinement by the highly correlated model chemistry used in this work, our mechanism, based on the initial reactive trajectory obtained from the *ab initio* nanoreactor of Das *et al.* seeking to satisfy a set of likely prebiotic conditions of temperature, absence of metal catalyst, *etc.*,[15] consists of a concerted water assisted reaction involving two water molecules in the transition state. For the gas phase, concerted, water assisted hydrolysis, Antonczak *et al.*[77] reported a Gibbs free energy of activation of 49.6 kcal mol^{-1} computed at the MP2/6-31G**//HF/3-21G level at 298 °C and 1 atm, which is consistent with our computed values, 50.5 kcal mol^{-1} (absolute)

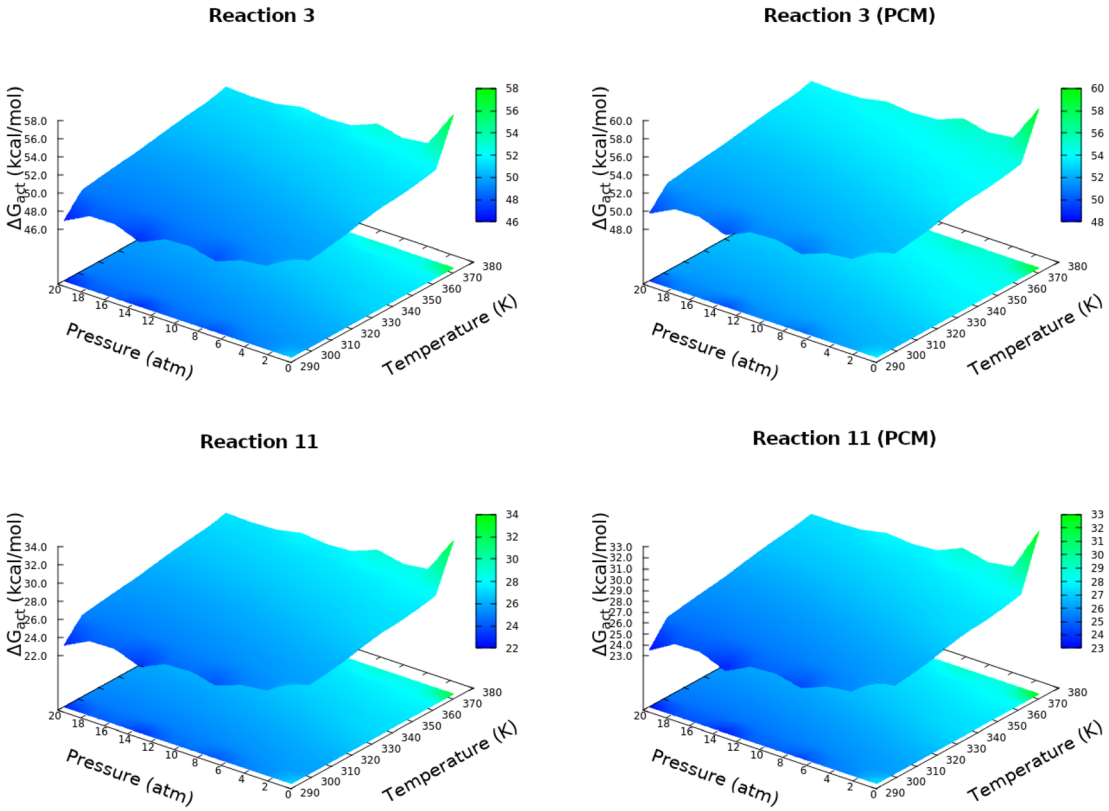

Fig. 1 Absolute activation energies for elementary steps **3** and **11** (Table 1), *in vacuo* (left) and in solution (right), over a grid of temperatures in [293, 373] K and pressures in [0.5, 20] atm.

and 45.7 kcal mol^{-1} (intrinsic). Later, using an improved theoretical framework (MP2/6-311+G**//B3LYP/6-31G*), Gorb *et al.*[78] studied the mechanism in solution through different solvent models considering, in all of them, five explicit water molecules. They obtained for the assisted concerted reaction, a Gibbs activation energy of 47.6 kcal mol^{-1} at the same conditions. Our mechanism in solution, computed with the substantially improved MP2/6-311++G(d, p) yields activation free energies of 53.2 kcal mol^{-1} (absolute) and 42.8 kcal mol^{-1} (intrinsic). The energies computed at 298 °C and 1 atm that we use to compare against previous studies are covered in the grids of temperature and pressure presented in Fig. S1 and S2†.

3.2 Dissection of the IRC

As stated in the Computational methods section, we chose reactions **3**, **10**, **11**, **12**, **17** from Table 1 to analyze the pivotal proton transfer processes as well as the breaking/formation of the all important C–C, C–N, C═O, and C–O bonds. The associated intermediates, transition states, and products are depicted in Fig. 2.

On the grounds of purely electronic energies, the profiles shown in Fig. 3 indicate that reactions **3**, **10** and **17** consume energy while reactions **11** and **12** release energy, however, Gibbs energies predict reaction **10** to be exergonic and reaction **12** to be endergonic. Notice that purely electronic energies describe only intrinsic processes (intermediate···products) while changes in Gibbs energies are calculated with the isolated reactants as reference. Thus, it is clear that in reaction **10**, accounting for entropy and internal degrees of freedom results in a strongly stabilized intermediate while in reaction **12** the intermediate is strongly destabilized. Table 1 reveals only slight changes in activation energies in going from gas phase to solution.

Most reactions involve large regions of structural changes before reaching the activated reactants, that is, ξ_R^* are far away from the reactants and comparatively closer to the transition states. The consequences for the reactions in the primitive Earth are that the environment needs to provide the means for the reactions to occur, in other words, that somewhat extreme conditions of temperature and pressure (especially temperature) are needed for the molecules to undergo the required structural changes leading to positive collision events. Transition states are neither earlier nor late, rather, transition state regions are well separated from reactants and products *via* large regions of *a priori* structural changes. Thus, as a general trend (there are exceptions), $|\Delta G^{\dagger}| > |\Delta G_{rxn}|$.

The reaction force, defined as the negative derivative of the potential energy with respect to the reaction coordinate along the reaction path provides a useful dissection of the entire mechanism: negative regions are associated with retarding forces while positive regions are associated with driving forces, thus, the local extrema of the force, corresponding to the second derivative of the IRC, or in other words, the inflection points of

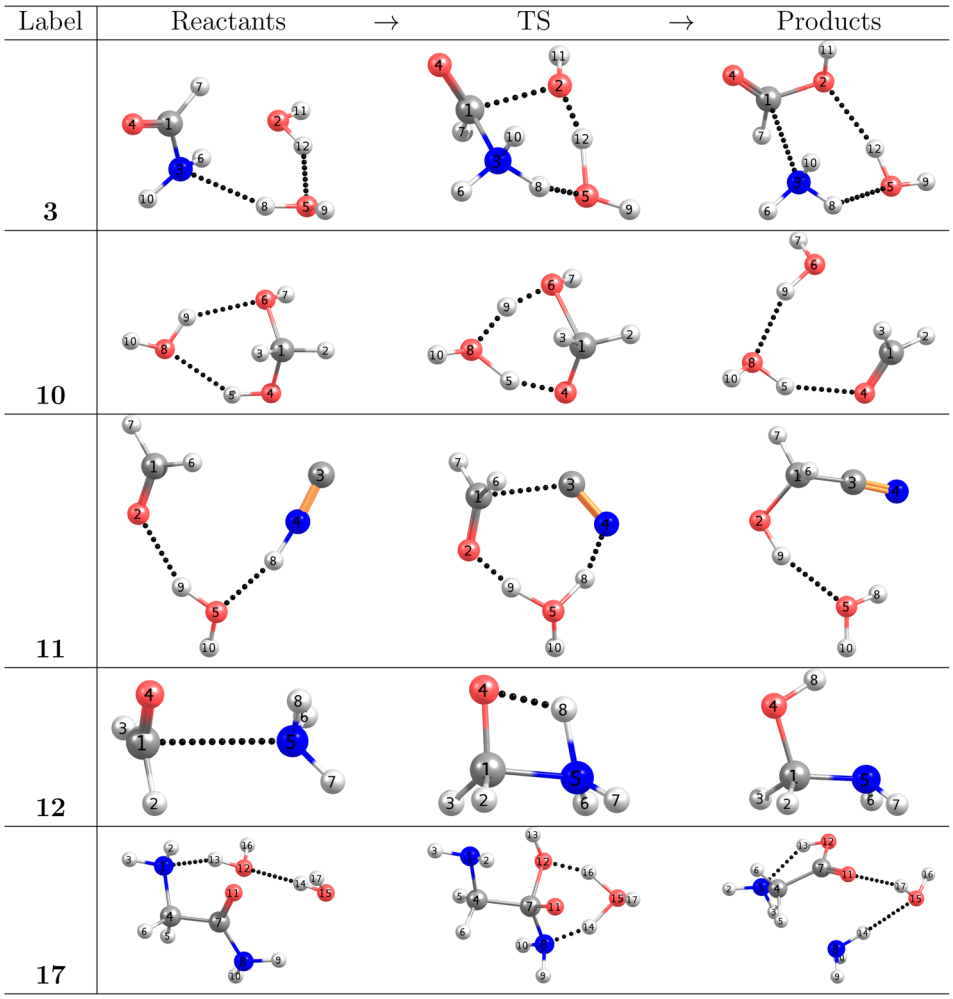

Fig. 2 Target elementary steps leading to the formation of formic acid (**3**), formaldehyde (**10**), glycolonitrile (**11**), methanolamine (**12**) and glycine (**17**). Intermolecular interactions are represented by dotted lines.

the IRC determine the progress of the chemical reaction as comprising a region of structural changes $\xi_R \rightarrow \xi_{R^*}$ opposing the chemical transformation, a region of mostly electronic rearrangements, $\xi_{R^*} \rightarrow \xi_{TS} \rightarrow \xi_{P^*}$ in which the force sharply switches from retarding (before TS) to driving (after TS), and a final structural relaxation $\xi_P \rightarrow \xi_{P^*}$ region that finally yields the corresponding products. There is an apparent inverse correlation between the length of the transition state region $\xi_{R^*} \rightarrow \xi_{TS} \rightarrow \xi_{P^*}$ and activation energies, namely, the smaller the TS region, the larger the activation energy. This observation is consistent with saying that larger activation energies are associated to larger TS regions, thus, most of the energy from the environment is transferred to the reacting system to overcome structural changes.

Steps **3** and **17** – both hydrolysis reactions – deviate from the typical behavior of the reaction force for an elementary step, characterized by a global maximum and global minimum connected through the transition state at $\xi = 0$. For these two reactions we observe two additional stationary points in the force plot, a local maximum and local minimum. This observation suggests that both reactions occur *via* a single, complex, concerted, borderline two-step mechanism, *i.e.*, there are two well differentiated regions along the IRC path where electronic activity predominates, and it also serves as an early indication of a formation/breaking of bonds taking place in a non-synchronous fashion. Further evidence for borderline two-step characterization of reactions **3**, **17** comes from the maximum of the chemical potential for both reactions in the region products, way past the transition state region. The electron flux plots accentuate the visualization of heavy electron activity outside the transition state region for reactions **3**, **17**, thus providing additional support for all the previous observations.

4 Evolution of bonding

4.1 Wiberg bond index, its derivative and synchronicity

The collection of plots in Fig. 4 reveals a picture of highly non synchronous concerted reactions. This is a striking observation because, except for reaction **12**, all other reactions involve double proton transfers, processes that are notoriously synchronous when they are the only chemical transformations.[79] However, that is not the case here since the

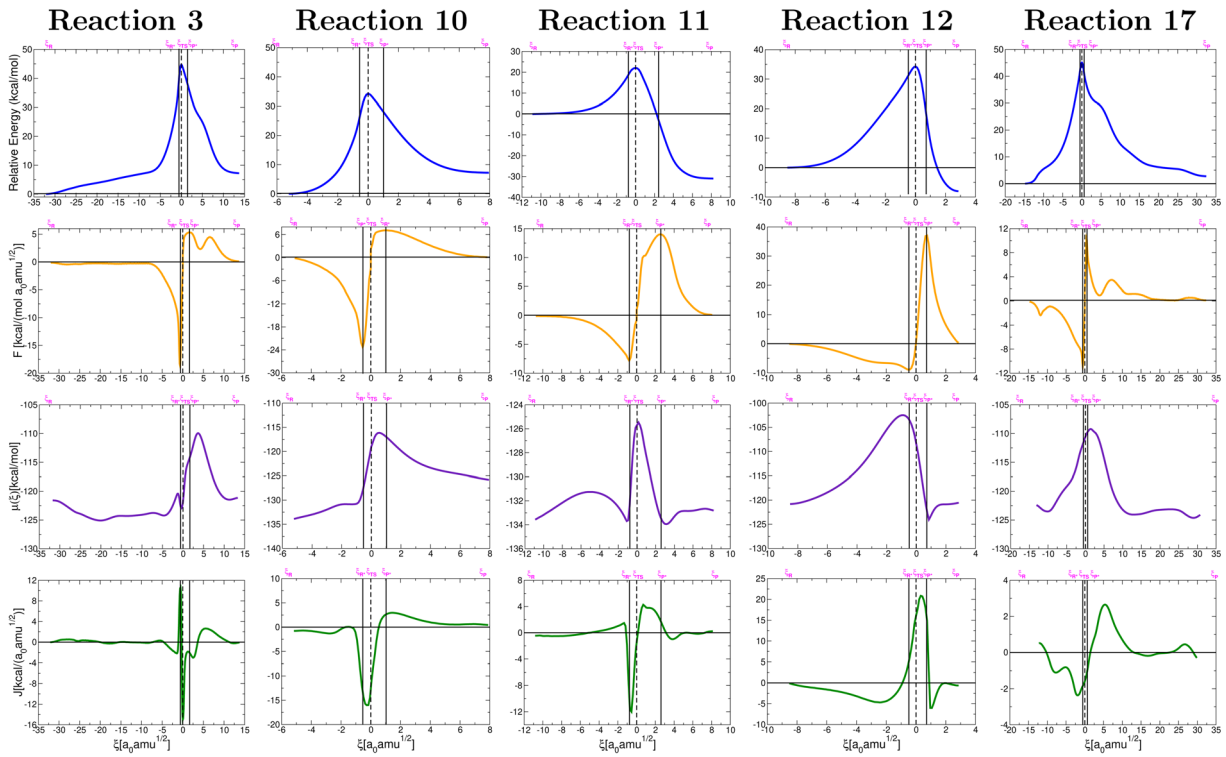

Fig. 3 Relative energies in the IRC (top row), reaction forces (second row), chemical potential (third row), and reaction electron flux (bottom row) corresponding to elementary steps leading to the formation of formic acid (reaction **3**, Fig. 2), formaldehyde (reaction **10**, Fig. 2), glycolonitrile (reaction **11**, Fig. 2), methanolamine (reaction **12**, Fig. 2) and glycine (reaction **17**, Fig. 2). Solid vertical lines define the reactants $\xi_R \rightarrow \xi_{R*}$, transition state $\xi_R \rightarrow \xi_{P*}$, and products $\xi_P \rightarrow \xi_{P*}$ regions. The position of the TS is marked by a dashed vertical line.

double proton transfers are accompanied, within the same concerted step, by breaking and formation of other largely covalent bonds. Remarkably, for all reactions involving double proton transfer, the formation and breaking of O–H bonds around a particular O atom occur in a synchronous fashion, apparently independently from other primitive processes (a small discrepancy occurs in reaction **11**).

For the set of five reactions shown in Fig. 2 a general mechanistic trend may be established from the plots in Fig. 4 in the context of a single step concerted reaction in each case. For the most part, the first process to initiate seems to be the double proton transfer in the reactions where they are present, then bond breaking/formation around the reactive carbon in the carbonyl group and finally rupture of the C–N bonds in the appropriate cases, which are the most reluctant to break. The reluctance of the C–N bond to break is clear from the fact that this rupture occurs far behind all other primitive processes, which have significantly progressed at the late stages of the reaction (this is true if reaction **12** is inverted). This is a pivotal point that highlights the importance of water not only as the medium in which all these reactions occur but also as a non innocent spectator catalyzing and actively taking part in most reactions (hydrogen atoms in water molecules end up in the products). In all cases, the double proton transfer process occurs mostly within the boundaries of the given TS region. Conversely, it is not uncommon for the breaking/formation of C–N, C–O, C=O and N–H bonds to anticipate or to extend beyond the TS region. In other words, besides the structural changes needed to bring reactants to the activated form and to deactivate the activated products, a sensible degree of electronic activity is still needed in the reactants and products regions.

Maximization of the chemical potential (Fig. 3) occurs ahead of the TS region for reaction **12** and beyond the TS region for reactions **3**, **17**. This is consistent with all descriptors in Fig. 4 which show high electron activity involved in the early formation of the C–N bond (reaction **12**) and in the late breaking of the C–N bond in reactions **3**, **17**. Reaction **10** is a well known dehydration reaction involving the transformation of methanediol into formaldehyde under the catalytic action of one water molecule that enables double proton transfer in our mechanism. This reaction deviates from other perfectly synchronous double proton transfers (*i.e.* in the dimer of formic acid[79]) because the two protons transferred in reaction **10** originate from different O–H bonds, C–O–H from methanediol and O–H from water.

4.2 Electron densities, virial ratios and NBO orbital interactions

The collection of plots in Fig. 5 provide a comprehensive picture of the evolution of the nature of bonding interactions for the set of reactions in Fig. 2, which is not only fully consistent with the conclusions drawn from the above analysis of the plots in Fig. 4 but also offers additional evidence and insight. All descriptors

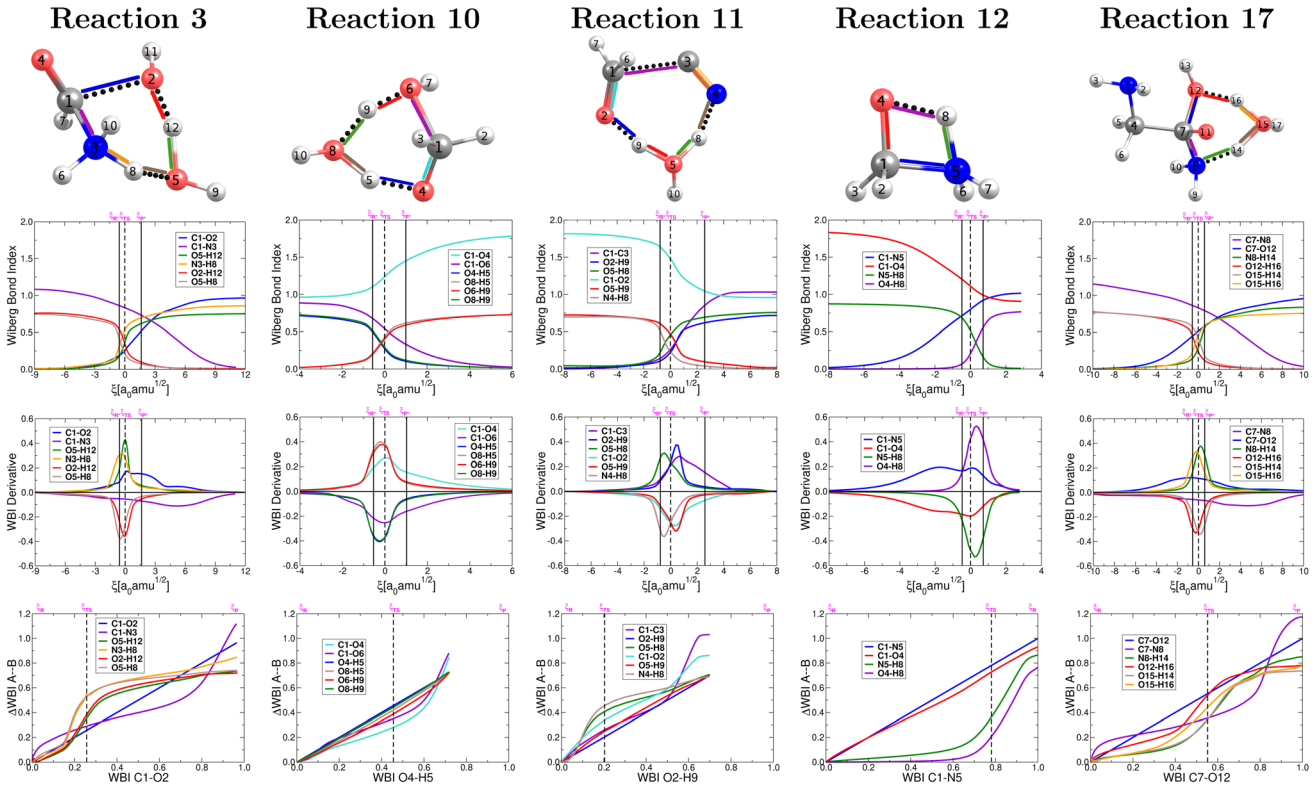

Fig. 4 Descriptors of the evolution of bonding as a function of the reaction coordinate for the one step concerted reactions leading to the formation of formic acid (reaction **3**, Fig. 2), formaldehyde (reaction **10**, Fig. 2), glycolonitrile (reaction **11**, Fig. 2), methanolamine (reaction **12**, Fig. 2) and glycine (reaction **17**, Fig. 2). Wiberg bond indexes (first row), their derivatives (second row) and GGR synchronicity[35] (third row). Solid vertical lines define the reactants $\xi_P \rightarrow \xi_{R*}$, transition state $\xi_R \rightarrow \xi_{P*}$, and products $\xi_P \rightarrow \xi_{P*}$ regions. The position of the TS is marked by a dashed vertical line.

are derived from the topological properties of the electron densities at bond critical points as afforded by QTAIM and by the shapes, overlap, and interaction energies in the donor → acceptor orbital paradigm as afforded by NBO.

Without a single exception, all broken/formed bonds are formally covalent, as characterized by virial ratios larger than 2 and large accumulations of electron density at bond critical points and by well defined σ, π bonds. This means that there are no ionic reactions and that all reactants and products have well defined bonds. As suggested above, hydrogen transfer seems to kick off the reacting system in the appropriate cases, that is, changes in electron density and virial ratios for the associated bonds seem to initiate ahead of all other primitive changes followed by the breaking/formation of C=O, C–O, and C–C bonds and mostly independent of the chemical transformation of C–N bonds.

In Fig. 5, bottom panel, all curves correspond to donor → acceptor interactions within the NBO paradigm. For those special cases in which a third lone pair on a given O atom arises, the corresponding interactions are followed *via* dotted lines. In general, breaking and formation of sigma bonds is due to a maximization in charge transfer following the $n_O \rightarrow \sigma^*$, $n_O \rightarrow \pi^*$, $n_N \rightarrow \sigma^*$, $n_N \rightarrow \pi^*$ rule. In agreement with all other descriptors, in the NBO context, both proton transfers occur very early during the reaction while the bonds associated with heavy atoms are transformed later within the same concerted step. Notice that for each one of the proton transfers, the formation of one σ_{O-H} orbital occurs simultaneously with the breaking of a second σ_{O-H} orbital associated with the transferred proton. Opposite to the double proton transfer, the bonds involving heavy atoms, *i.e.*, formation of C1–O2 and breaking of C1–N3, do not occur simultaneously. In fact, the formation of the σ_{C1-O2} is completed at the activated products coordinate and precedes the breaking of σ_{C1-N3}, which is not finalized until the very end of the reaction, at the coordinate of the products. Although after the reaction has taken place the $\pi_{C1=O4}$ orbital remains intact, it is by no means (just like the catalytic water) an innocent spectator for the reaction to occur: reorganizing its electron density is essential during the $\xi_{TS} \rightarrow \xi_{P*}$ interval in which a $\pi \rightarrow \sigma$ transformation occurs, inducing the subsequent breaking of the C1–N3 orbital followed by the restoring of the $\pi_{C1=O4}$ orbital in the formic acid of the final products.

5 General description of the mechanism of reaction 3

It is worth emphasizing two important factors at this point of our discussion. First, each one of the 23 reactions in Table 1 (including those in Fig. 2), occurs *via* a one step concerted

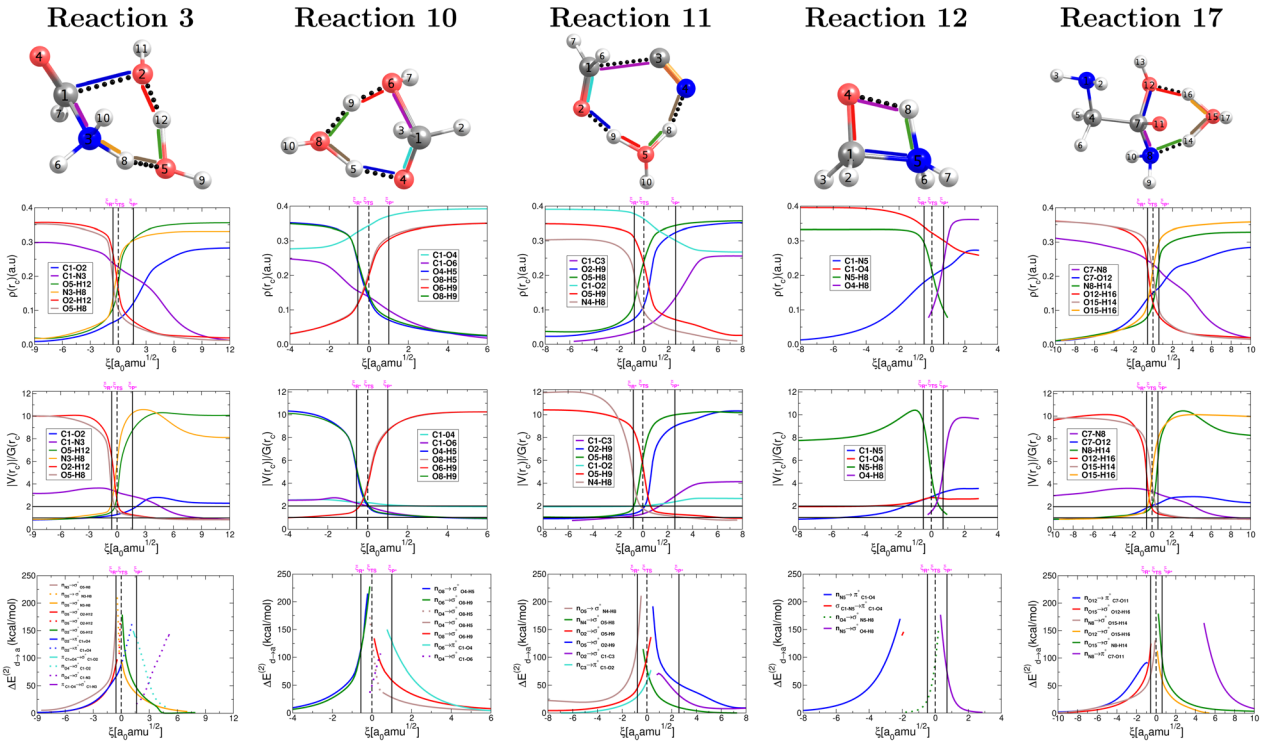

Fig. 5 Descriptors of the evolution of bonding as a function of the reaction coordinate for the one step concerted reactions leading to the formation of formic acid (reaction **3**, Fig. 2), formaldehyde (reaction **10**, Fig. 2), glycolonitrile (reaction **11**, Fig. 2), methanolamine (reaction **12**, Fig. 2) and glycine (reaction **17**, Fig. 2). Electron densities at bond critical points (first row), virial ratios at bond critical points (second row), and representative intermolecular donor → acceptor orbital interactions (third row). Solid vertical lines define the reactants $\xi_R \rightarrow \xi_{R*}$, transition state $\xi_R \rightarrow \xi_{P*}$, and products $\xi_{P*} \rightarrow \xi_P$ regions. The position of the TS is marked by a dashed vertical line.

process, that is, all the primitive changes we are about to discuss occur during the same step. Second, although the previous QTAIM, NBO analyses detail the mechanism for reactions **3**, **10**, **11**, **12**, **17**, all the features and conclusions are mostly transferable to all other reactions because they involve the formation and breaking of the same types of bonds under the same conditions. Accordingly, we provide next a detailed mechanistic sequence of the events leading to the formation of formaldehyde and ammonia from formamide and two water molecules along the lines of reaction **3** (Fig. 2). In addition to the descriptors of the evolution of bonding interactions provided in Fig. 4, 5, further evidence to support our claims is found in Fig. 6, which follows the specific orbitals involved in the intermolecular interactions resulting in the breaking/formation of bonds during the course of reaction **3**. As a reference to compare the strength of intermolecular interactions, we recall the values for the archetypal H–O···H–O hydrogen bond in the water dimer:[80,81] $E_{da}^{(2)} = -7.09$ kcal mol^{-1}, $\rho(\mathbf{r}_c) = 2.3 \times 10^{-2}$ a.u., $|\nu(\mathbf{r}_c)|/\mathscr{G}(\mathbf{r}_c) = 0.89$, where $\mathbf{r}_c$ stands for the bond critical point. The general features for the formation of formic acid (FA) and ammonia (A) from formamide (F1) and two water molecules (W1, W2) are summarized in Scheme 2.

As discussed before, every single reaction begins by forming a stabilized long range complex, ξ_R in Scheme 2. ξ_R is the starting point of the one step concerted reaction. In the case of reaction **3**, this complex involves two specific intermolecular hydrogen bonds of strengths comparable to the isolated water dimer: H–N···H–O $E_{da}^{(2)} = -4.75$ kcal mol^{-1}, $\rho(\mathbf{r}_c) = 1.7 \times 10^{-2}$ a.u, $|\nu(\mathbf{r}_c)|/\mathscr{G}(\mathbf{r}_c) = 0.88$ in F1···W1, and H–O···H–O $E_{da}^{(2)} = -6.51$ kcal mol^{-1}, $\rho(\mathbf{r}_c) = 2.4 \times 10^{-2}$ a. u, $|\nu(\mathbf{r}_c)|/\mathscr{G}(\mathbf{r}_c) = 0.90$ in W1···W2. The formation of these complexes leads to somewhat shallow, purely electronic energy wells which may be overcome simply by correcting for the ZPE energies or by accounting for temperature, entropy, and internal degrees of freedom (*i.e.*, using Gibbs energies) as concluded above during the discussion of the energetics of the reaction profiles. The formation of these complexes requires minimal distortion of the electron densities from the isolated reactants, and thus the shallow wells. The regions within the IRC are conveniently analyzed in a separate fashion as follows:

$\xi_R \rightarrow \xi_{R*}$ region: two important developments characterize this region: first, somewhere within this interval (at $\xi = -14.97$ a_0 a.m.u$^{1/2}$), a critical point for the C1···O2 interaction appears, this interaction strengthens steadily up to the coordinate of the activated reactants, however, not at the same rate as the interactions involved in the double proton transfer as consistently shown by all synchronicity, QTAIM, and NBO descriptors in Fig. 4, 5 and 6, respectively. Second, all orbital interactions associated to intermolecular contacts increase by large factors (from 4.75 to 185.35 kcal mol^{-1}, *etc.*, Fig. 6). These observations are consistent with the sensible structural changes needed to accommodate all reacting fragments in the positions required

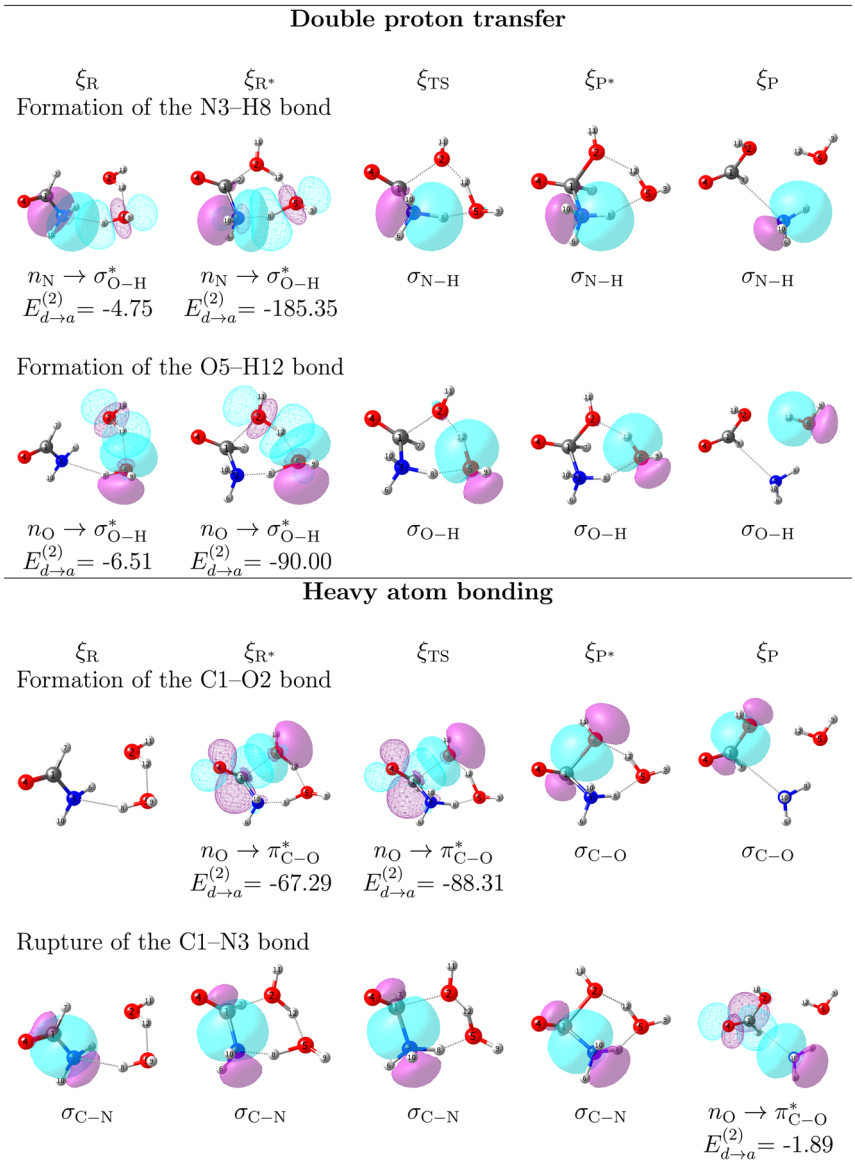

Fig. 6 Orbital interactions leading to the breaking/formation of bonds driving the production of formic acid and ammonia from formamide and two water molecules along the lines of the one step, concerted mechanism of reaction **3** (Fig. 2). All donor → acceptor interaction energies in kcal mol^{-1}.

for the reaction to occur. Notice that although structural changes dominate this region of the IRC, it is not void of electronic activity.

$\xi_{R^*} \rightarrow \xi_{TS}$ region: the double proton transfer is so early for this reaction that both protons have completely migrated at ξ_{TS}. Multiple evidence supports this claim: virial ratios larger than 2 thus indicating covalent bonding ($|\nu(\mathbf{r}_c)|/\mathcal{G}(\mathbf{r}_c) = 5.84$ for σ_{N3-H8} and $|\nu(\mathbf{r}_c)|/\mathcal{G}(\mathbf{r}_c) = 2.92$ for σ_{O5-H12}), large bond orders, and the clear presence of well defined σ_{N-H}, σ_{O-H} orbitals for the newly formed bonds (Fig. 6). This reorganization of the electron density yields formal negative and positive charges at O2 and N3 respectively (Scheme 2), which are major players driving the progress of the reaction beyond the TS. The asynchronous character of this reaction is clearly seen in the fact that up to ξ_{TS}, two O–H bonds have been broken, one O–H and one N–H bond have been formed, while C1⋯O2 remains a long range contact and C1–N3 remains a well defined σ bond (for additional support, see the evolution of all bonds in the GGR synchronicity index, bottom panel in Fig. 4).

$\xi_{TS} \rightarrow \xi_{P^*}$ region: this region is mostly devoted to the formation of the σ_{C1-O2} bond *via* a classic nucleophilic attack from the negatively charged H–O:− to the carbon atom in the carbonyl group. The formation of the σ_{C1-O2} bond results in a reorganization of the electron density of the C=O bond to produce a formally charged C–O− fragment (Scheme 2), beautifully supported by the emergence of a third lone pair on the carbonyl oxygen (O4) right at (ξ_{P^*}). There is a progressive weakening of the soon to be broken C–N bond in going from ξ_{TS} to (ξ_{P^*}) as seen in the steady decrease of the bond order, electron density, and virial ratio.

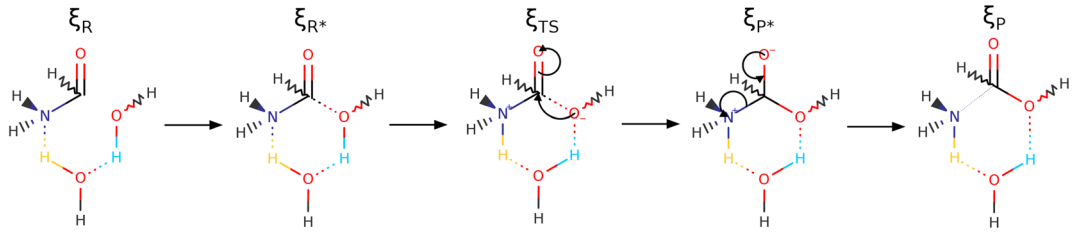

Scheme 2 Reaction mechanism covering the entire $\xi_R \rightarrow \xi_{R^*} \rightarrow \xi_{TS} \rightarrow \xi_{P^*} \rightarrow \xi_P$ IRC, as dissected by the reaction force (Fig. 3), for the one step concerted formation of formic acid from formamide and two water molecules. Notice that one of the water molecules is incorporated into the final formic acid and that the other is not an innocent spectator as indicated by the colors associated to the double proton transfer. See Fig. S3 in the ESI† to follow the natural charges at all oxygen atoms justifying the assignment of formal negative charges at specific points.

$\xi_{P^*} \rightarrow \xi_P$ Region: this step involves separation of the fragments, restoring of the $\pi_{C=O}$ bond, and final rupture of the C1–N3 bond to liberate ammonia and formic acid. Evidence for the rupture of the C1–N3 bond: the virial ratio goes from 2.92 (covalent bond) to 0.82 (long range interaction); the bond order goes from 0.73 to 0.03; the derivative of the bond order decreases substantially; the σ_{C1-N3} orbital ceases to exist; a lone pair is formed in N3. The driving force for the breaking of the C1–N3 bond is unveiled by NBO in the form of $n_{O4} \rightarrow \sigma^*_{C1-N3}$ destabilizing charge transfer from the formally charged C–O$^-$ fragment freshly formed at (ξ_{P^*}), as clearly shown by the dotted purple line at the leftmost bottom panel in Fig. 6. Notice that the breaking of the C1–N3 bond occurs very late in the reaction, way past the activated products, just beyond the point in which the C1=O4 carbonyl is restored and the third lone pair is no longer available after doing its job of weakening C1–N3.

6 Connection to prebiotic chemistry

We now venture an analysis of our results in the context of prebiotic chemistry. Albert Szent-Györgi famously stated that "Life is nothing but an electron looking for a place to rest". This argument may be readily applied to essential processes for the sustainability of life, such as oxidative metabolism. What we can see from our work and from the scientific literature[15,82] is that this argument may be extended to prebiotic chemistry as well. Indeed, the set of 23 reactions studied here was not designed with any purpose in mind, rather, they were obtained from *ab initio* nanoreactors fed with HCN and water by Das and coworkers,[15] nonetheless, they constitute a progressive network of oxidation reactions from the beginning to the actual production of carbon dioxide, formaldehyde, formic acid, formaldimine, glycolaldehyde, glycine, glycolonitrile, oxazole derivatives, *etc.*, and could be seen as a set of "electron accumulator processes". Another important aspect in our calculations is that water does not simply act as the medium in which all reactions occur, but in many instances, besides working as a catalyst and a non-innocent spectator, it is actually involved in the chemical reactions to the point that water atoms end up in the products. HCN is thought to have existed both in the oceans and in the atmosphere, which also contained water vapor, gratifyingly, the reactions studied here have shown to be plausible in both phases.

Until the discovery of the actual causes and mechanisms of the origin of life, we may assert in a pragmatic although speculative way, that a set of conditions are necessary. Namely, a network of chemical reactions capable of producing the building blocks of the molecules of life (such as the ones studied in this work) in local environments that further facilitate their combination to produce large molecules of such astonishing diversity and complexity as proteins and DNA. Our calculations unveil only moderate changes in activation energies as a function of pressure and temperature for the set of reactions studied here (Fig. 1, S1 and S2†), this observation supports the perspective of life just exposed because given the current poor understanding of the conditions of the Hadean earth, these small changes in reaction barriers indicate that above those thresholds, the chemical reactions producing the building blocks for the molecules of life will occur under a wide variety of conditions. The local favorable environments are the product of large scale cumulative changes in the course of billions of years brought about by deterministic molecular processes, that is, chemical reactions, and the consequential physical and chemical changes of the environment (slow building of a tolerable atmosphere, regulation of temperatures and acidic conditions, *etc.*) that allow the emergence and evolution of life under a particular set of local environmental evolution pressures.

The ever increasing entropy of the universe, as stated by the second law of thermodynamics, is the ultimate reason behind the molecular scale evolution (deterministic, not random, because of the need to satisfy the equilibration of chemical potentials in reacting systems) that changes the chemical landscape and then the environment itself. A second factor contributing to the increase in entropy of the universe in the process of originating life is the complexity of the multitude of reaction channels accessible to produce the small molecules needed to make large biomolecules, as is clearly the case in the present work. Furthermore, proteins are built upon primary sequences of just 20 amino acids, thus, there are on the order of 2.4×10^{18} possible different primary sequences for even the smallest proteins.[83] Under this perspective, any local environment (a planet, a moon, or regions within) capable of undergoing the necessary changes under periods of time long enough to avoid major catastrophes caused by external agents, is poised to originate and sustain life. There is a high probability that

once set in motion, many of these evolution patterns may not succeed in creating life, but by virtue of the immense dimensions of our observable universe, the emergence of life is not only deterministic, but should be a rather common place.

7 Conclusions

The reaction mechanisms for a set of 23 reactions leading to the formation of carbon dioxide, formaldehyde, formic acid, formaldimine, glycolaldehyde, glycine, glycolonitrile, and oxazole derivatives, among other precursors of large biomolecules in gas phase and in solution are presented in this work. All reactions occur *via* single step highly non synchronous processes. Given the presence of the substrates and of large amounts of water in the early Earth oceans and atmosphere,[84,85] it is highly likely that this set of prebiotic reactions took place in the primitive Earth and should have been rather common. Indeed, relatively high energy barriers are obtained in each case, however, the role of catalysts (clays, icy surfaces, *etc.*), the different sources of energy associated with the likely prebiotic conditions of the primitive earth, such as oceans with temperatures between 80–100 °C,[15,86] shock heating,[87] vulcanism, electric discharges, impacts of extraterrestrial objects,[88] among others, cannot be ignored as potential triggers for these networks of reactions and may account for the need for significant concentrations of these building blocks for the subsequent formation of larger biomolecules to be effective. The set of 23 reactions studied here constitutes a progressive network of oxidation reactions from the beginning to the actual production of the precursors of large biomolecules. Our results are consistent with the finding of Das *et al.*[15] in that in many cases, water does not act simply as the medium in which all reactions occur, working not just as a catalyst or as an innocent spectator, but it is actually involved in the chemical reactions to the point that water atoms end up in the products.

Conflicts of interest

There are no conflicts to declare.

Acknowledgements

Internal support from Universidad de Antioquia *via* "Estrategia para la sostenibilidad" is acknowledged. J. A. M. L. was supported by a grant from ANID (FONDECYT Regular 1221936), Chile.

References

1 J. D. Sutherland, The origin of life—out of the blue, *Angew. Chem., Int. Ed.*, 2016, **55**, 104–121.
2 B. Palmer, A review on the spontaneous formation of the building blocks of life and the generation of a set of hypotheses governing universal abiogenesis, *Int. J. Astrobiol.*, 2013, **12**, 39–44.
3 A. Pérez-Villa, F. Pietrucci and A. M. Saitta, Prebiotic chemistry and origins of life research with atomistic computer simulations, *Phys. Life Rev.*, 2020, **34**, 105–135.
4 M. W. Powner and J. D. Sutherland, Prebiotic chemistry: a new modus operandi, *Philos. Trans. R. Soc., B*, 2011, **366**, 2870–2877.
5 J. L. Bada, New insights into prebiotic chemistry from Stanley Miller's spark discharge experiments, *Chem. Soc. Rev.*, 2013, **42**, 2186–2196.
6 A. Lazcano and S. L. Miller, The origin and early evolution of life: prebiotic chemistry, the pre-RNA world, and time, *Cell*, 1996, **85**, 793–798.
7 L. E. Orgel, The origin of life—a review of facts and speculations, *Trends Biochem. Sci.*, 1998, **23**, 491–495.
8 H. J. Cleaves, Prebiotic chemistry: what we know, what we don't, *Evol.: Educ. Outreach*, 2012, **5**, 342–360.
9 C. Jeancolas, C. Malaterre and P. Nghe, Thresholds in origin of life scenarios, *Iscience*, 2020, **23**, 101756.
10 M. Tessera, Is pre-Darwinian evolution plausible?, *Biol. Direct*, 2018, **13**, 1–18.
11 E. O. Leslie, Prebiotic chemistry and the origin of the RNA world, *Crit. Rev. Biochem. Mol. Biol.*, 2004, **39**, 99–123.
12 T. R. Cech, The RNA worlds in context, *Cold Spring Harbor Perspect. Biol.*, 2012, **4**, a006742.
13 A. Jandura and H. M. Krause, The new RNA world: growing evidence for long noncoding RNA functionality, *Trends Genet.*, 2017, **33**, 665–676.
14 R. Krishnamurthy, Giving rise to life: transition from prebiotic chemistry to protobiology, *Acc. Chem. Res.*, 2017, **50**, 455–459.
15 T. Das, S. Ghule and K. Vanka, Insights into the origin of life: Did it begin from HCN and H_2O?, *ACS Cent. Sci.*, 2019, **5**, 1532–1540.
16 A. Tokunaga, S. Beck, T. Geballe, J. Lacy and E. Serabyn, The detection of HCN on Jupiter, *Icarus*, 1981, **48**, 283–289.
17 S. Aalto, S. Garcia-Burillo, S. Muller, J. Winters, P. Van Der Werf, C. Henkel, F. Costagliola and R. Neri, Detection of HCN, HCO+, and HNC in the Mrk 231 molecular outflow-Dense molecular gas in the AGN wind, *Astron. Astrophys.*, 2012, **537**, A44.
18 E. Lellouch, M. Gurwell, B. Butler, T. Fouchet, P. Lavvas, D. Strobel, B. Sicardy, A. Moullet, R. Moreno, D. Bockelée-Morvan, *et al.*, Detection of CO and HCN in Pluto's atmosphere with ALMA, *Icarus*, 2017, **286**, 289–307.
19 B. Fegley, R. G. Prinn, H. Hartman and G. H. Watkins, Chemical effects of large impacts on the Earth's primitive atmosphere, *Nature*, 1986, **319**, 305–308.
20 J. P. Ferris and W. J. Hagan Jr, HCN and chemical evolution: the possible role of cyano compounds in prebiotic synthesis, *Tetrahedron*, 1984, **40**, 1093–1120.
21 A. W. Schwartz, A. Voet and M. Van der Veen, Recent progress in the prebiotic chemistry of HCN, *Origins Life*, 1984, **14**, 91–98.
22 C. N. Matthews, *Origins*, Springer, 2004; pp pp 121–135.
23 S. Nandi, D. Bhattacharyya and A. Anoop, Prebiotic chemistry of HCN tetramerization by automated reaction search, *Chem.–Eur. J.*, 2018, **24**, 4885–4894.

24 R. F. Bader, A quantum theory of molecular structure and its applications, *Chem. Rev.*, 1991, **91**, 893–928.
25 P. L. Popelier, *Atoms in Molecules: An Introduction*, Prentice Hall, London, 2000.
26 S. J. Grabowski, What Is the Covalency of Hydrogen Bonding?, *Chem. Rev.*, 2011, **111**, 2597–2625.
27 A. E. Reed, L. A. Curtiss and F. Weinhold, Intermolecular interactions from a natural bond orbital, donor-acceptor viewpoint, *Chem. Rev.*, 1988, **88**, 899–926.
28 F. Weinhold and C. R. Landis, *Discovering Chemistry with Natural Bond Orbitals*, Wiley-VCH, Hoboken NJ, 2012, p. 319.
29 E. D. Glendening, C. R. Landis and F. Weinhold, Natural bond orbital methods, *Wiley Interdiscip. Rev.: Comput. Mol. Sci.*, 2012, **2**, 1–42.
30 S. Gómez, A. Restrepo and C. Hadad, Theoretical tools to distinguish O-ylides from O-ylidic complexes in carbene–solvent interactions, *Phys. Chem. Chem. Phys.*, 2015, **17**, 31917–31930.
31 S. Gomez, D. Guerra, J. G. Lopez, A. Toro-Labbe and A. Restrepo, A detailed look at the reaction mechanisms of substituted carbenes with water, *J. Phys. Chem. A*, 2013, **117**, 1991–1999.
32 P. Tobón, S. Gomez, A. Restrepo and F. Núñez-Zarur, Role of Substrate Substituents in Alkene Metathesis Mediated by a Ru Alkylidene Catalyst, *Organometallics*, 2021, **40**, 119–133.
33 P. Farfán, S. Gómez and A. Restrepo, Dissection of the Mechanism of the Wittig Reaction, *J. Inorg. Chem.*, 2019, **84**, 14644–14658.
34 P. Farfán, S. Gómez and A. Restrepo, On the origins of stereoselectivity in the Wittig reaction, *Chem. Phys. Lett.*, 2019, **728**, 153–155.
35 C. Giraldo, S. Gómez, F. Weinhold and A. Restrepo, Insight into the Mechanism of the Michael Reaction, *ChemPhysChem*, 2016, **17**, 2022–2034.
36 S. Gómez, H. Ramírez-Malule, W. Cardona-G, E. Osorio and A. Restrepo, Double-ring epimerization in the biosynthesis of clavulanic acid, *J. Phys. Chem. A*, 2020, **124**, 9413–9426.
37 S. Gómez, E. Osorio, E. Dzib, R. Islas, A. Restrepo and G. Merino, Revisiting the Rearrangement of Dewar Thiophenes, *Molecules*, 2020, **25**, 284.
38 B. Mennucci, Polarizable continuum model, *Wiley Interdiscip. Rev.: Comput. Mol. Sci.*, 2012, **2**, 386–404.
39 J. Tomasi, B. Mennucci and R. Cammi, Quantum Mechanical Continuum Solvation Models, *Chem. Rev.*, 2005, **105**, 2999–3094.
40 A. Toro-Labbé, S. Gutiérrez-Oliva, M. C. Concha, J. S. Murray and P. Politzer, Analysis of two intramolecular proton transfer processes in terms of the reaction force, *J. Chem. Phys.*, 2004, **121**, 4570–4576.
41 A. Toro-Labbé, S. Gutiérrez-Oliva, J. Murray and P. Politzer, A new perspective on chemical and physical processes: the reaction force, *Mol. Phys.*, 2007, **105**, 2619–2625.
42 J. Martínez and A. Toro-Labbé, The reaction force. A scalar property to characterize reaction mechanisms, *J. Math. Chem.*, 2009, **45**, 911–927.
43 S. Gómez, D. Guerra, J. G. López, A. Toro-Labbé and A. Restrepo, A Detailed Look at the Reaction Mechanisms of Substituted Carbenes with Water, *J. Phys. Chem. A*, 2013, **117**, 1991–1999.
44 R. G. Parr, *Horizons of quantum chemistry*, Springer, 1980, pp 5–15.
45 R. G. Parr and Z. Zhou, Absolute hardness: unifying concept for identifying shells and subshells in nuclei, atoms, molecules, and metallic clusters, *Acc. Chem. Res.*, 1993, **26**, 256–258.
46 E. Echegaray and A. Toro-Labbé, Reaction electronic flux: a new concept to get insights into reaction mechanisms. Study of model symmetric nucleophilic substitutions, *J. Phys. Chem. A*, 2008, **112**, 11801–11807.
47 M. L. Cerón, E. Echegaray, S. Gutiérrez-Oliva, B. Herrera and A. Toro-Labbé, The reaction electronic flux in chemical reactions, *Sci. China: Chem.*, 2011, **54**, 1982–1988.
48 C. Morell, V. Tognetti, E. Bignon, E. Dumont, N. Hernandez-Haro, B. Herrera, A. Grand, S. Gutierrez-Oliva, L. Joubert, A. Toro-Labbé, *et al.*, Insights into the chemical meanings of the reaction electronic flux, *Theor. Chem. Acc.*, 2015, **134**, 1–7.
49 N. Rojas-Valencia, S. Gómez, D. Guerra and A. Restrepo, A detailed look at the bonding interactions in the microsolvation of monoatomic cations, *Phys. Chem. Chem. Phys.*, 2020, **22**, 13049–13061.
50 M. J. Frisch; G. W. Trucks; H. B. Schlegel; G. E. Scuseria; M. A. Robb; J. R. Cheeseman; G. Scalmani; V. Barone; B. Mennucci; G. A. Petersson *et al.*, *Gaussian 09 Revision E.01*, Gaussian Inc., Wallingford CT, 2009.
51 T. Keith, *AIMALL (version 13.05.06)*, TK Gristmill Software, Overland Park KS, USA, 2013, **http://aim.tkgristmill.com**.
52 E. D. Glendening, J. K. Badenhoop, A. E. Reed, J. E. Carpenter, J. A. Bohmann, C. M. Morales, C. R. Landis and F. Weinhold, *NBO 6.0*, Theoretical Chemistry Institute, University of Wisconsin, Madison, 2013.
53 J. F. Kasting and T. P. Ackerman, Climatic consequences of very high carbon dioxide levels in the Earth's early atmosphere, *Science*, 1986, **234**, 1383–1385.
54 D. P. Summers and S. Chang, Prebiotic ammonia from reduction of nitrite by iron (II) on the early Earth, *Nature*, 1993, **365**, 630–633.
55 J. W. Valley, W. H. Peck, E. M. King and S. A. Wilde, A cool early Earth, *Geology*, 2002, **30**, 351–354.
56 P. von Paris, H. Rauer, J. L. Grenfell, B. Patzer, P. Hedelt, B. Stracke, T. Trautmann and F. Schreier, Warming the early Earth-CO_2 reconsidered, *Planet. Space Sci.*, 2008, **56**, 1244–1259.
57 J. F. Kasting and M. T. Howard, Atmospheric composition and climate on the early Earth, *Philos. Trans. R. Soc., B*, 2006, **361**, 1733–1742.
58 L. Song and J. Kästner, Formation of the prebiotic molecule NH_2CHO on astronomical amorphous solid water surfaces: accurate tunneling rate calculations, *Phys. Chem. Chem. Phys.*, 2016, **18**, 29278–29285.
59 Y. Yung and M. McElroy, Fixation of nitrogen in the prebiotic atmosphere, *Science*, 1979, **203**, 1002–1004.
60 V. Barone, C. Latouche, D. Skouteris, F. Vazart, N. Balucani, C. Ceccarelli and B. Lefloch, Gas-phase formation of the

prebiotic molecule formamide: insights from new quantum computations, *Mon. Not. R. Astron. Soc.: Lett.*, 2015, **453**, L31–L35.

61 P. V. Coveney, J. B. Swadling, J. A. Wattis and H. C. Greenwell, Theory, modelling and simulation in origins of life studies, *Chem. Soc. Rev.*, 2012, **41**, 5430–5446.

62 J. Hao, M. Mokhtari, U. Pedreira-Segade, L. J. Michot and I. Daniel, Transition metals enhance the adsorption of nucleotides onto clays: Implications for the origin of life, *ACS Earth Space Chem.*, 2018, **3**, 109–119.

63 C. Ponnamperuma, A. Shimoyama and E. Friebele, Clay and the origin of life, *Origins Life*, 1982, **12**, 9–40.

64 A. Rimola, M. Sodupe and P. Ugliengo, Role of mineral surfaces in prebiotic chemical evolution. *In silico* quantum mechanical studies, *Life*, 2019, **9**, 10.

65 J. Krug, P. Popelier and R. Bader, Theoretical study of neutral and of acid and base-promoted hydrolysis of formamide, *J. Phys. Chem.*, 1992, **96**, 7604–7616.

66 J. Krissansen-Totton, G. N. Arney and D. C. Catling, Constraining the climate and ocean pH of the early Earth with a geological carbon cycle model, *Proc. Natl. Acad. Sci. U. S. A.*, 2018, **115**, 4105–4110.

67 J. L. Bada, C. Bigham and S. L. Miller, Impact melting of frozen oceans on the early Earth: implications for the origin of life, *Proc. Natl. Acad. Sci. U. S. A.*, 1994, **91**, 1248–1250.

68 A. W. Schwartz, H. Joosten and A. Voet, Prebiotic adenine synthesis *via* HCN oligomerization in ice, *Biosystems*, 1982, **15**, 191–193.

69 J. L. Bada, How life began on Earth: a status report, *Earth Planet. Sci. Lett.*, 2004, **226**, 1–15.

70 C. Menor-Salván and M. R. Marín-Yaseli, Prebiotic chemistry in eutectic solutions at the water–ice matrix, *Chem. Soc. Rev.*, 2012, **41**, 5404–5415.

71 J. W. Gauld, H. Audier, J. Fossey and L. Radom, Water-catalyzed interconversion of conventional and distonic radical cations: methanol and methyleneoxonium radical cations, *J. Am. Chem. Soc.*, 1996, **118**, 6299–6300.

72 J. W. Gauld and L. Radom, Effects of neutral bases on the isomerization of conventional radical cations $CH_3X^{\bullet}$ + to their distonic isomers $^{\bullet}CH_2X$+ H (X= F, OH, NH_2): Proton-transport catalysis and other mechanisms, *J. Am. Chem. Soc.*, 1997, **119**, 9831–9839.

73 A. Rimola, M. Sodupe and P. Ugliengo, Deep-space glycine formation *via* Strecker-type reactions activated by ice water dust mantles. A computational approach, *Phys. Chem. Chem. Phys.*, 2010, **12**, 5285–5294.

74 S. Antonczak, M. Ruiz-López and J.-L. Rivail, The hydrolysis mechanism of formamide revisited: comparison between *ab initio*, semiempirical and DFT results, *J. Mol. Model.*, 1997, **3**, 434–442.

75 T. Oie, G. H. Loew, S. K. Burt, J. S. Binkley and R. D. MacElroy, Quantum chemical studies of a model for peptide bond formation: formation of formamide and water from ammonia and formic acid, *J. Am. Chem. Soc.*, 1982, **104**, 6169–6174.

76 J. H. Jensen, K. K. Baldridge and M. S. Gordon, Uncatalyzed peptide bond formation in the gas phase, *J. Phys. Chem.*, 1992, **96**, 8340–8351.

77 S. Antonczak, M. Ruiz-Lopez and J. Rivail, Ab initio analysis of water-assisted reaction mechanisms in amide hydrolysis, *J. Am. Chem. Soc.*, 1994, **116**, 3912–3921.

78 L. Gorb, A. Asensio, I. Tuñón and M. F. Ruiz-López, The mechanism of formamide hydrolysis in water from *ab initio* calculations and simulations, *Chem.–Eur. J.*, 2005, **11**, 6743–6753.

79 P. Farfán, A. Echeverri, E. Diaz, J. D. Tapia, S. Gómez and A. Restrepo, Dimers of formic acid: Structures, stability, and double proton transfer, *J. Chem. Phys.*, 2017, **147**, 044312.

80 S. Gómez, N. Rojas-Valencia, S. A. Gómez, C. Cappelli, G. Merino and A. Restrepo, A molecular twist on hydrophobicity, *Chem. Sci.*, 2021, **12**, 9233–9245.

81 L. Uribe, S. Gómez, T. Giovannini, F. Egidi and A. Restrepo, An efficient and robust procedure to calculate absorption spectra of aqueous charged species applied to NO_2^-, *Phys. Chem. Chem. Phys.*, 2021, **23**, 14857–14872.

82 J. Ferris, J. Wos, T. Ryan, A. Lobo and D. Donner, Biomolecules from HCN, *Origins Life*, 1974, **5**, 153–157.

83 J. David, S. Gómez, D. Guerra, D. Guerra and A. Restrepo, A Comprehensive Picture of the Structures, Energies, and Bonding in the Alanine Dimers, *ChemPhysChem*, 2021, **22**, 2401–2412.

84 M. Ferus, P. Kubelík, A. Knížek, A. Pastorek, J. Sutherland and S. Civiš, High energy radical chemistry formation of HCN-rich atmospheres on early Earth, *Sci. Rep.*, 2017, **7**, 1–9.

85 J. L. Bada and H. J. Cleaves, Ab initio simulations and the Miller prebiotic synthesis experiment, *Proc. Natl. Acad. Sci. U. S. A.*, 2015, **112**, E342.

86 J. W. Morse and F. T. Mackenzie, Hadean ocean carbonate geochemistry, *Aquat. Geochem.*, 1998, **4**, 301–319.

87 H. Follmann and C. Brownson, Darwin's warm little pond revisited: from molecules to the origin of life, *Naturwissenschaften*, 2009, **96**, 1265–1292.

88 Y. Furukawa, T. Sekine, M. Oba, T. Kakegawa and H. Nakazawa, Biomolecule formation by oceanic impacts on early Earth, *Nat. Geosci.*, 2009, **2**, 62–66.